

Interplay between charge order and superconductivity in the kagome metal KV_3Sb_5

Feng Du,^{1,2,*} Shuaishuai Luo,^{1,2,*} Brenden R. Ortiz,³ Ye Chen,^{1,2} Weiyin Duan,^{1,2}
Dongting Zhang,^{1,2} Xin Lu,^{1,2} Stephen D. Wilson,³ Yu Song,^{1,2,†} and Huiqiu Yuan^{1,2,4,‡}

¹Center for Correlated Matter and Department of Physics, Zhejiang University, Hangzhou 310058, China

²Zhejiang Province Key Laboratory of Quantum Technology and Device,

Department of Physics, Zhejiang University, Hangzhou 310058, China

³Materials Department and California Nanosystems Institute,

University of California Santa Barbara, Santa Barbara, CA, 93106, United States

⁴State Key Laboratory of Silicon Materials, Zhejiang University, Hangzhou 310058, China

The kagome metal KV_3Sb_5 hosts charge order, topologically nontrivial Dirac band crossings, and a superconducting ground state with unconventional characteristics, providing an ideal platform to investigate the interplay between different electronic states on the kagome lattice. Here we study the evolution of charge order and superconductivity in KV_3Sb_5 under hydrostatic pressure using electrical resistivity measurements. With the application of pressure, the superconducting transition temperature $T_c = 0.9$ K under ambient pressure quickly increases to 3.1 K at $p = 0.4$ GPa, as charge order progressively weakens. Upon further increasing pressure, signatures of charge order disappears at $p_{c1} \approx 0.5$ GPa and T_c is gradually suppressed, forming a superconducting dome that terminates at $p \approx 10$ GPa. Beyond $p \approx 10$ GPa, a second superconducting dome emerges with maximum $T_c \approx 1.0$ K at $p_{c2} \approx 22$ GPa, which becomes fully suppressed at $p \approx 28$ GPa. The suppression of superconductivity for the second superconducting dome is associated with the appearance of a unique high-pressure phase, possibly a distinct charge order.

The kagome lattice provides a rich setting to realize exotic states of matter, including quantum spin liquids [1–3], topologically nontrivial electronic structures [4–6] and collective electronic orders [7–11]. Recently, discovery of the two-dimensional kagome metal series AV_3Sb_5 ($A = K, Rb, Cs$) [12–15] sparked immense interest, as they exhibit topological band structures, sizable correlation effects, charge order and superconductivity. This series further exhibits a giant anomalous Hall effect in the absence of magnetism [13, 16, 17], which is proposed to result from an unconventional charge order with chiral character [18, 19]. While the superconducting pairing symmetry remains unclear, multiple superconducting domes were revealed under applied pressure in CsV_3Sb_5 [20, 21], which may result from distinct and possibly unconventional superconducting states. These results make AV_3Sb_5 an ideal platform to investigate the relationship between charge order and superconductivity on the kagome lattice.

The interplay between charge order and superconductivity may come in different forms, shown schematically in Fig. 1. Since charge order and superconductivity compete for the same electronic density of states at the Fermi level, the superconducting transition temperature T_c is typically enhanced as charge order is suppressed, and evolves more gradually beyond the full suppression of charge order, as depicted in Fig. 1(a) [22–24]. Alternatively, quantum critical fluctuations associated with charge order may play a dominant role, with a superconducting dome emerging around the quantum critical point, accompanied by a fan of non-Fermi-liquid behavior [Fig. 1(b)], similar to unconventional superconductivity around magnetic or nematic quantum critical points

[25–28]. Although signatures for such an interplay have been suggested [29–31], it remains far from being well-established. As most studies on the interplay between superconductivity and charge order focused on conventional superconductors, it becomes important to examine the corresponding behaviors in systems with unconventional characteristics, such as the AV_3Sb_5 series. In addition, as the AV_3Sb_5 series exhibits multiple Fermi surfaces [13], it may be susceptible to pressure-induced changes in the electronic structure and electron-phonon interactions, which may promote electronic instabilities distinct from the ambient pressure charge order, allowing for a more nuanced interplay between different order parameters.

In this work, we study the temperature-pressure phase diagram of KV_3Sb_5 single crystals through electrical transport measurements. We find T_c increases from 0.9 K to 3.1 K at 0.4 GPa, with the low-pressure charge order (LPCO) becoming indiscernible above $p_{c1} \approx 0.5$ GPa. T_c is then gradually suppressed with increasing pressure and terminates at $p \approx 10$ GPa, forming a highly asymmetric superconducting dome. A second superconducting dome appears at higher pressures, reaching a maximum $T_c \approx 1.0$ K at $p_{c2} \approx 22$ GPa. Upon further increase of pressure, a high-pressure phase (HPP) distinct from the LPCO appears, evidenced by a hysteretic anomaly in resistivity. Concomitant with appearance of the HPP, superconductivity is suppressed with increasing pressure and disappears above $p \approx 28$ GPa. Our observations suggest a nontrivial evolution of the electronic structure and the electron-phonon interaction under pressure, with qualitatively different intrinsic resistivity up to room temperature correlated with distinct

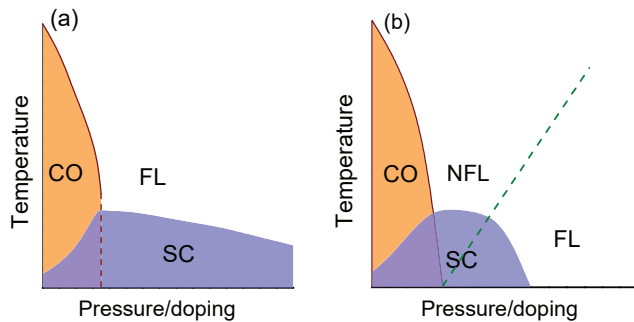


Figure 1: Schematic phase diagrams of the interplay between charge order and superconductivity (a) where the two orders compete, and (b) when quantum fluctuations associated with charge order are dominant, leading to a fan of non-Fermi-liquid behavior. The orange shaded region corresponds to charge order (CO), and the purple shaded region corresponds to superconductivity (SC). In the normal state without charge order, the system may exhibit Fermi liquid (FL) or non-Fermi-liquid (NFL) behavior.

ground states. These findings highlight the AV_3Sb_5 series as a host for tuning between distinct electronic instabilities, and indicate the interplay of superconductivity with the LPCO and the HPP to be mainly driven by their competition, with quantum critical fluctuations playing a minimal role.

Single crystals of KV_3Sb_5 were grown using a self-flux method, with physical properties under ambient pressure reported previously [14]. While K-deficiencies may be utilized to achieve unusual transport behaviors [32], they also significantly increase residual resistivity and suppress superconductivity [12]. Therefore, detailed characterization was performed to ensure that our samples exhibit minimal K-deficiencies [33]. Electrical resistivity measurements under pressure were carried out using a piston-cylinder cell (PCC) and a diamond anvil cell (DAC), with Daphne oil 7373 or silicon oil as the pressure medium to ensure hydrostaticity of our measurements [33].

Measurements of the electrical resistivity $\rho(T)$ with pressures up to 2.3 GPa are shown in Fig. 2(a), with the corresponding $d\rho/dT$ curves shown in Fig. 2(d). A clear anomaly associated with T_{CO} can be seen at 0.1 GPa, and as pressure is increased up to 0.4 GPa, the anomaly clearly moves to lower temperatures, before becoming indiscernible at 0.5 GPa. These results imply that charge order associated with T_{CO} disappears rapidly upon pressure-tuning. It should be noted that the resistivity anomaly associated with T_{CO} is weaker in KV_3Sb_5 compared to CsV_3Sb_5 , and it further weakens upon the application of pressure. As the strength of the resistivity anomaly reflects the size of the underlying electronic order parameter, this suggests that in addition to the suppression of T_{CO} , the magnitude of the LPCO is also reduced under pressure in KV_3Sb_5 .

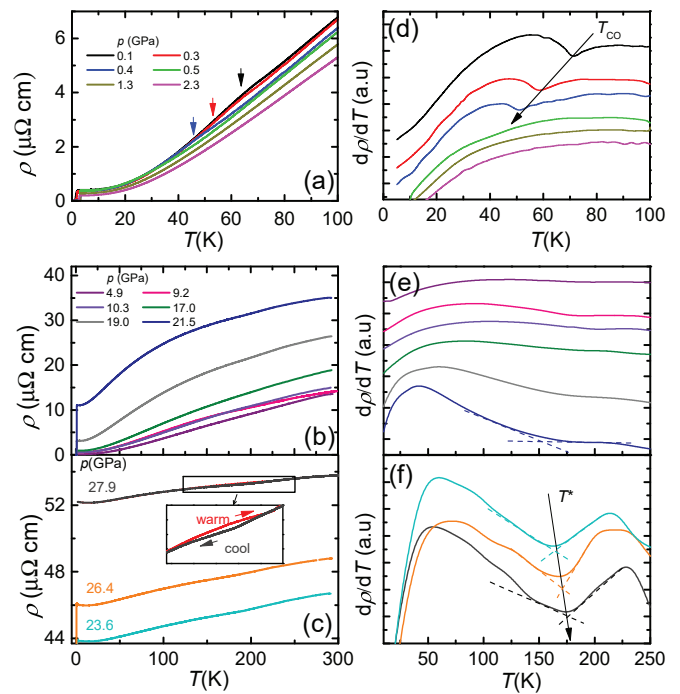


Figure 2: In-plane resistivity $\rho(T)$ of KV_3Sb_5 under pressures from (a) 0.1 to 2.3 GPa, (b) 4.9 to 21.5 GPa and (c) 23.6 to 27.9 GPa. The corresponding $d\rho(T)/dT$ are respectively shown in (d), (e) and (f). Data in (a) are measured in a piston-cylinder cell, and data in (b) and (c) are measured in a diamond anvil cell. Aside from the one $\rho(T)$ curve at 27.9 GPa which is measured upon warming, all data are taken upon cooling. The inset in (c) zooms into the temperature region with hysteretic resistivity at 27.9 GPa.

The electrical resistivity $\rho(T)$ in the pressure range 4.9 GPa to 21.5 GPa are shown in Fig. 2(b), with the corresponding $d\rho/dT$ curves shown in Fig. 2(e). In combination with results in Fig. 2(d), it can be seen that $d\rho/dT$ does not exhibit clear anomalies from 0.5 GPa to 19 GPa, suggesting no detectable electronic orders that compete with superconductivity in this pressure range. $\rho(T)$ for pressure from 23.6 GPa to 27.9 GPa are shown in Fig. 2(c), with the corresponding $d\rho/dT$ curves shown in Fig. 2(f). For these pressures, a clear dip is observed in $d\rho/dT$, which increases in temperature with increasing pressure. Furthermore, the corresponding anomaly in $\rho(T)$ exhibits a clear hysteresis upon cooling and warming [inset of Fig. 2(c)], indicating the anomaly to be associated with a HPP appearing via a first-order phase transition. The HPP's hysteretic nature, significantly higher onset temperature T^* , and the increase of T^* with increasing pressure all indicate the HPP to be distinct from the LPCO. Moreover, $\rho(T)$ in the pressure regime with the HPP is qualitatively different from those in Figs. 2(a) and (b), exhibiting a much reduced $\delta\rho = \rho(300\text{ K}) - \rho_0$ (ρ_0 being the resistivity just above the onset of superconductivity). A similar anomaly in $d\rho/dT$ is also ob-

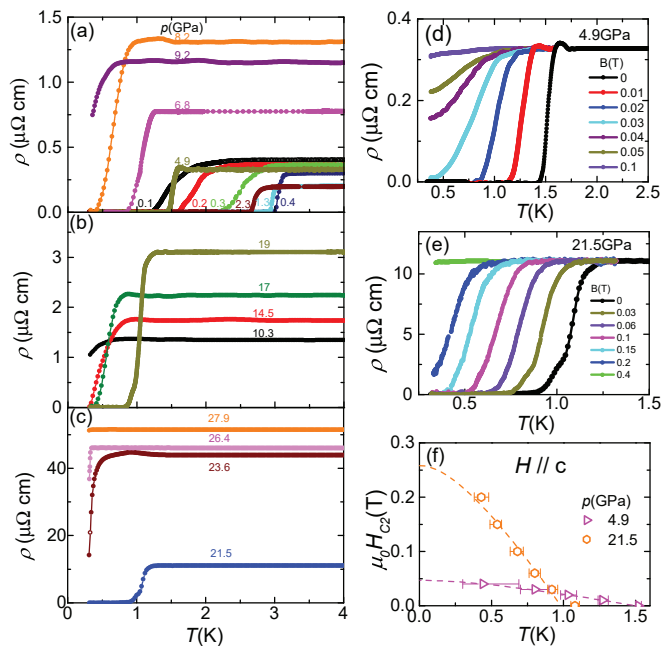


Figure 3: In-plane resistivity $\rho(T)$ of KV_3Sb_5 under pressures from (a) 0.1 to 9.2 GPa, (b) 10.3 to 19 GPa and (c) 21.5 to 27.9 GPa, zoomed in for $T \leq 4$ K. Low-temperature resistivity $\rho(T)$ under various c -axis magnetic fields for (d) 4.9 GPa and (e) 21.5 GPa. (f) The upper critical field of KV_3Sb_5 as a function of temperature under 4.9 GPa and 21.5 GPa. Fits to the WHH model are shown as dashed lines.

served at 21.5 GPa in Fig. 2(e), pointing to appearance of the HPP already at 21.5 GPa. However, the anomaly is much less prominent at this pressure, and $\rho(T)$ exhibits a larger $\delta\rho$, different from behaviors in Fig. 2(c). This suggests that appearance of the HPP is first-order-like upon pressure-tuning, with the HPP partially stabilized over the sample volume at 21.5 GPa. We note that ρ_0 appears anomalously large at high pressures, which could be related to structural defects of the sample, possibly caused by structural distortions associated with the HPP and the increased susceptibility to sample fracturing under high pressures.

Figs. 3(a)-(c) zooms into $\rho(T)$ for $T \leq 4$ K, focusing on the evolution of superconductivity upon pressure-tuning. As can be seen, T_c increases with increasing pressure up to 0.4 GPa, then decreases slowly at higher pressures and becomes strongly suppressed at 9.2 GPa [Fig. 3(a)], forming a highly asymmetric superconducting dome with maximal T_c near the border of the LPCO. Upon further increase of pressure, T_c is first enhanced with increasing pressure from 10.3 to 19 GPa [Fig. 3(b)], and then decreases from 21.5 to 27.9 GPa [Fig. 3(c)], forming a second superconducting dome.

To probe the superconducting state associated with the two superconducting domes, we measured resistivity under an applied magnetic field along the c -axis at 4.9 GPa and 21.5 GPa, respectively shown in Figs. 3(d)

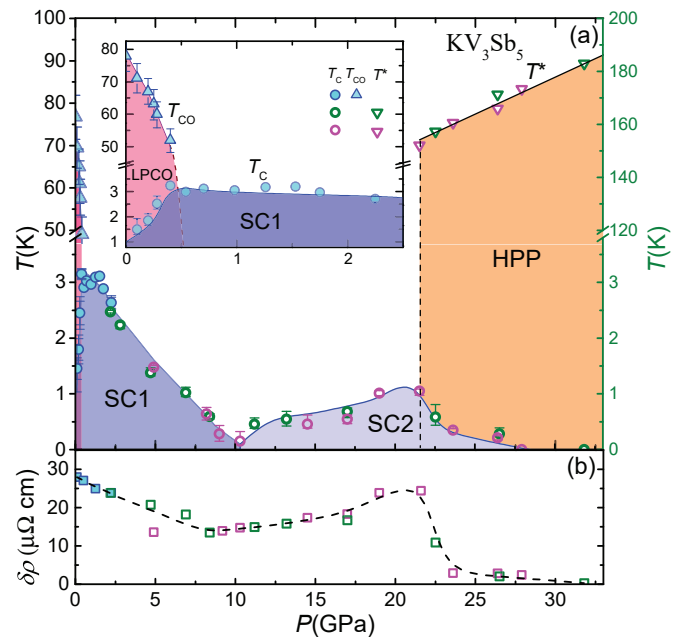


Figure 4: (a) The temperature-pressure phase diagram of KV_3Sb_5 . Two superconducting regions (SC1 and SC2), the low-pressure charge order (LPCO) and the high-pressure phase (HPP) can be identified in the figure. The inset zooms into the low pressure region, highlighting the interplay between superconductivity and the LPCO. (b) Pressure dependence of the electrical resistivity change $\delta\rho = \rho(300 \text{ K}) - \rho_0$. The solid line is a guide-to-the-eye. Full symbols correspond to points obtained using a PCC, and empty symbols correspond to points obtained using a DAC. For measurements using a DAC, two samples were studied [33] and are presented using different symbols.

and (e). The upper critical fields $\mu_0 H_{c2}(T)$ are determined as when $\rho(T)$ drops to $\rho_0/2$, and are summarized in Fig. 3(f). $\mu_0 H_{c2}(T)$ could be fit with the Werthamer-Helfand-Hohenberg (WHH) model [34] for both pressures, with fits shown in Fig. 3(f). As can be seen, although $T_c \approx 1.5$ K at 4.9 GPa is higher than $T_c \approx 1.0$ K at 21.5 GPa, superconductivity is suppressed much more quickly under an applied field at 4.9 GPa, pointing to a significant pressure-tuning of the superconducting state not captured by T_c . This point is also highlighted by a nontrivial evolution of the upper critical field around the LPCO [33].

The phase diagram obtained from electrical resistivity measurements under pressure is shown in Fig. 4(a), with T_c determined from when $\rho(T)$ drops to $\rho_0/2$, T_{CO} from the $d\rho(T)/dT$ dip in Fig. 2(d), and T^* from the $d\rho/dT$ dip in Fig. 2(f). In cases where superconductivity onsets but does not drop to $\rho_0/2$ at the lowest measured temperature, $\rho(T)$ is extrapolated to obtain an estimate of T_c . The phase diagram reveals that while T_c is enhanced from 0.9 K under ambient pressure to 3.1 K at $p_{c1} \approx 0.5$ GPa (4.4 K/GPa), the decrease above p_{c1} is much more grad-

ual, with the superconducting dome terminating at $p \approx 10$ GPa (≈ -0.30 K/GPa). Such an asymmetric superconducting dome is empirically different from the case of superconductivity emerging near a quantum critical point. Combined with the persistence of Fermi-liquid behavior up to at least 17 GPa [33], our results suggest that competition between superconductivity and the LPCO is mainly responsible for the maximum in T_c at the border of the LPCO. A similar mechanism may also account for the T_c maxima at $p_{c2} \approx 22$ GPa, given the HPP appears in a clear first-order fashion. Therefore, despite the unusual temperature-pressure phase diagram with the HPP, and unconventional features associated with the LPCO, the interplay between superconductivity with both the LPCO and the HPP seem to be dominated by a competition mechanism [Fig. 1(a)], in contrast to a scenario involving quantum criticality [Fig. 1(b)].

On the other hand, the strong suppression of superconductivity at $p \approx 10$ GPa likely involves a significant modification to the electronic structure or electron-phonon interactions, leading to a clear kink in the pressure-evolution of $\delta\rho$, shown in Fig. 4(b). Since $\delta\rho$ results from electron-electron and electron-phonon scattering and is insensitive to impurity or crystal defects, the kink in $\delta\rho$ at $p \approx 10$ GPa may result from a Lifshitz transition [35, 36] or a non-monotonic evolution of the electron-phonon interactions, which in turn naturally accounts for distinct characters of the LPCO and the HPP stabilized on the two sides of $p \approx 10$ GPa. Moreover, $\delta\rho$ reduces sharply near p_{c2} where the HPP is stabilized, consistent with the HPP being a novel state distinct from the LPCO, and supports its first-order appearance with increasing pressure.

Insensitivity of the HPP to applied magnetic field [33], its clear signature in resistivity, and presence of thermal hysteresis suggests the HPP may correspond to a charge ordered state or an altered structural phase. In either case, pressure-tuning of the electronic structure and electron-phonon interactions should play a pivotal role in stabilizing the HPP under pressure, whose exact nature needs to be clarified by further experiments. The observation of the second superconducting dome having maximal T_c around $p_{c2} \approx 22$ GPa where the HPP appears, suggests a possible role of the HPP in formation of the second superconducting dome. However, the origin of the second superconductivity dome, whether it exhibits a distinct pairing symmetry relative to the first dome, and exact relationship to the HPP, need to be addressed in future works. It is interesting to note that a similar second superconducting dome is also observed in CsV_3Sb_5 under pressure [20, 36], although superconductivity remains robust up to 100 GPa, compared to KV_3Sb_5 in which superconductivity is suppressed around 28 GPa. The origin of such a significant difference between the two systems calls for further studies, with focus on whether a HPP can be stabilized in CsV_3Sb_5 under pressure and the role of

hydrostaticity in determining the temperature-pressure phase diagram.

The temperature-pressure phase diagram we uncover in KV_3Sb_5 contains two distinct superconducting domes, both with optimal superconductivity near the border of a competing electronic order. Such a behavior is highly unconventional, reminiscent of the heavy fermion superconductor CeCu_2Si_2 [26], where one superconducting dome is associated with a magnetic quantum critical point and the other with a first-order valence instability. In contrast, the first superconducting dome in KV_3Sb_5 is associated with an highly unusual charge order, and the second with a new high-pressure phase that is possibly a distinct charge order. Furthermore, compared to the evolution of superconductivity near the border of the LPCO in KV_3Sb_3 , CsV_3Sb_5 exhibits an additional superconducting dome well inside the LPCO regime [21]. These rich behaviors in AV_3Sb_5 suggest the presence of multiple electronic instabilities proximate in energy, with the balance between them determined sensitively by the electronic structure, electron-phonon interactions and dimensionality ($c/a = 1.633$ in KV_3Sb_5 and 1.694 in CsV_3Sb_5), highlighting the kagome lattice as an ideal platform for both realizing and manipulating novel states of quantum matter.

In conclusion, we studied the temperature-pressure phase diagram of the kagome metal KV_3Sb_5 under hydrostatic pressure, and observed two superconducting domes, with the first exhibiting a competition between superconductivity and the low-pressure charge order, and the second associated with a unique high-pressure phase. Our findings suggest pressure significantly modifies the electronic structure and electron-phonon interactions, leading to the nuanced evolution of physical properties and phases under pressure. Despite the nontrivial evolution of superconductivity with pressure, the interplay between charge order and superconductivity is most likely dominated by their competition. Our results evidence two superconducting domes and distinct electronic orders stabilized in the kagome metal KV_3Sb_5 , setting the stage for exploring superconductivity on the kagome lattice in the presence of distinct collective electronic orders, and constraining models that capture charge order and superconductivity in the AV_3Sb_5 series.

This work was supported by the National Key R&D Program of China (No. 2017YFA0303100, No. 2016YFA0300202), the Key R&D Program of Zhejiang Province, China (2021C01002), the National Natural Science Foundation of China (No. 11974306 and No. 12034017), the Science Challenge Project of China (No. TZ2016004), and the Fundamental Research Funds for the Central Universities of China. S.D.W. and B.R.O. gratefully acknowledge support via the UC Santa Barbara NSF Quantum Foundry funded via the Q-AMASE-i program under award DMR-1906325. B.R.O. also acknowledges support from the California NanoSystems In-

stitute through the Elings fellowship program.

* These authors contributed equally to this work.

† Electronic address: yusong_phys@zju.edu.cn

‡ Electronic address: hqyuan@zju.edu.cn

- [1] I. Syozi, *Progress of Theoretical Physics* **6**, 306 (1951), URL <https://doi.org/10.1143/ptp/6.3.306>.
- [2] T.-H. Han, J. S. Helton, S. Chu, D. G. Nocera, J. A. Rodriguez-Rivera, C. Broholm, and Y. S. Lee, *Nature* **492**, 406 (2012), URL <https://doi.org/10.1038/nature11659>.
- [3] C. Broholm, R. J. Cava, S. A. Kivelson, D. G. Nocera, M. R. Norman, and T. Senthil, *Science* **367**, eaay0668 (2020), URL <https://doi.org/10.1126/science.aay0668>.
- [4] L. Ye, M. Kang, J. Liu, F. von Cube, C. R. Wicker, T. Suzuki, C. Jozwiak, A. Bostwick, E. Rotenberg, D. C. Bell, et al., *Nature* **555**, 638 (2018), URL <https://doi.org/10.1038/nature25987>.
- [5] E. Liu, Y. Sun, N. Kumar, L. Muechler, A. Sun, L. Jiao, S.-Y. Yang, D. Liu, A. Liang, Q. Xu, et al., *Nature Physics* **14**, 1125 (2018), URL <https://doi.org/10.1038/s41567-018-0234-5>.
- [6] M. Kang, L. Ye, S. Fang, J.-S. You, A. Levitan, M. Han, J. I. Facio, C. Jozwiak, A. Bostwick, E. Rotenberg, et al., *Nature Materials* **19**, 163 (2019), URL <https://doi.org/10.1038/s41563-019-0531-0>.
- [7] W.-S. Wang, Z.-Z. Li, Y.-Y. Xiang, and Q.-H. Wang, *Physical Review B* **87** (2013), URL <https://doi.org/10.1103/physrevb.87.115135>.
- [8] S. V. Isakov, S. Wessel, R. G. Melko, K. Sengupta, and Y. B. Kim, *Physical Review Letters* **97** (2006), URL <https://doi.org/10.1103/physrevlett.97.147202>.
- [9] H.-M. Guo and M. Franz, *Physical Review B* **80** (2009), URL <https://doi.org/10.1103/physrevb.80.113102>.
- [10] M. L. Kiesel, C. Platt, and R. Thomale, *Physical Review Letters* **110** (2013), URL <https://doi.org/10.1103/physrevlett.110.126405>.
- [11] J. Wen, A. Rüegg, C.-C. J. Wang, and G. A. Fiete, *Physical Review B* **82** (2010), URL <https://doi.org/10.1103/physrevb.82.075125>.
- [12] B. R. Ortiz, L. C. Gomes, J. R. Morey, M. Winiarski, M. Bordelon, J. S. Mangum, I. W. H. Oswald, J. A. Rodriguez-Rivera, J. R. Neilson, S. D. Wilson, et al., *Physical Review Materials* **3** (2019), URL <https://doi.org/10.1103/physrevmaterials.3.094407>.
- [13] B. R. Ortiz, S. M. Teicher, Y. Hu, J. L. Zuo, P. M. Sarte, E. C. Schueller, A. M. Abeykoon, M. J. Krogstad, S. Rosenkranz, R. Osborn, et al., *Physical Review Letters* **125** (2020), URL <https://doi.org/10.1103/physrevlett.125.247002>.
- [14] B. R. Ortiz, P. M. Sarte, E. M. Kenney, M. J. Graf, S. M. L. Teicher, R. Seshadri, and S. D. Wilson, *Physical Review Materials* **5** (2021), URL <https://doi.org/10.1103/physrevmaterials.5.034801>.
- [15] Q. Yin, Z. Tu, C. Gong, Y. Fu, S. Yan, and H. Lei, *Chinese Physics Letters* **38**, 037403 (2021), URL <https://doi.org/10.1088/0256-307x/38/3/037403>.
- [16] S.-Y. Yang, Y. Wang, B. R. Ortiz, D. Liu, J. Gayles, E. Derunova, R. Gonzalez-Hernandez, L. Šmejkal, Y. Chen, S. S. P. Parkin, et al., *Science Advances* **6**, eabb6003 (2020), URL <https://doi.org/10.1126/sciadv.abb6003>.
- [17] E. M. Kenney, B. R. Ortiz, C. Wang, S. D. Wilson, and M. J. Graf, *Journal of Physics: Condensed Matter* **33**, 235801 (2021), URL <https://doi.org/10.1088/1361-648x/abe8f9>.
- [18] Y.-X. Jiang, J.-X. Yin, M. M. Denner, N. Shumiya, B. R. Ortiz, J. He, X. Liu, S. S. Zhang, G. Chang, I. Belopolski, et al. (2020), arXiv:2012.15709.
- [19] F. H. Yu, T. Wu, Z. Y. Wang, B. Lei, W. Z. Zhuo, J. J. Ying, and X. H. Chen (2021), arXiv:2102.10987.
- [20] C. C. Zhao, L. S. Wang, W. Xia, Q. W. Yin, J. M. Ni, Y. Y. Huang, C. P. Tu, Z. C. Tao, Z. J. Tu, C. S. Gong, et al. (2021), arXiv:2102.08356.
- [21] K. Y. Chen, N. N. Wang, Q. W. Yin, Z. J. Tu, C. S. Gong, J. P. Sun, H. C. Lei, Y. Uwatoko, and J. G. Cheng (2021), arXiv:2102.09328.
- [22] A. M. Gabovich, A. I. Voitenko, J. F. Annett, and M. Ausloos, *Superconductor Science and Technology* **14**, R1 (2001), URL <https://doi.org/10.1088/0953-2048/14/4/201>.
- [23] B. Shen, F. Du, R. Li, A. Thamizhavel, M. Smidman, Z. Y. Nie, S. S. Luo, T. Le, Z. Hossain, and H. Q. Yuan, *Physical Review B* **101** (2020), URL <https://doi.org/10.1103/physrevb.101.144501>.
- [24] F. Du, H. Su, S. S. Luo, B. Shen, Z. Y. Nie, L. C. Yin, Y. Chen, R. Li, M. Smidman, and H. Q. Yuan, *Physical Review B* **102** (2020), URL <https://doi.org/10.1103/physrevb.102.144510>.
- [25] N. D. Mathur, F. M. Grosche, S. R. Julian, I. R. Walker, D. M. Freye, R. K. W. Haselwimmer, and G. G. Lonzarich, *Nature* **394**, 39 (1998), URL <https://doi.org/10.1038/27838>.
- [26] H. Q. Yuan, F. M. Grosche, M. Deppe, C. Geibel, G. Sparn, and F. Steglich, *Science* **302**, 2104 (2003), URL <https://doi.org/10.1126/science.1091648>.
- [27] T. Shibauchi, A. Carrington, and Y. Matsuda, *Annual Review of Condensed Matter Physics* **5**, 113 (2014), URL <https://doi.org/10.1146/annurev-conmatphys-031113-133921>.
- [28] H.-H. Kuo, J.-H. Chu, J. C. Palmstrom, S. A. Kivelson, and I. R. Fisher, *Science* **352**, 958 (2016), URL <https://doi.org/10.1126/science.aab0103>.
- [29] T. Gruner, D. Jang, Z. Huesges, R. Cardoso-Gil, G. H. Fecher, M. M. Koza, O. Stockert, A. P. Mackenzie, M. Brando, and C. Geibel, *Nature Physics* **13**, 967 (2017), URL <https://doi.org/10.1038/nphys4191>.
- [30] L. E. Klintberg, S. K. Goh, P. L. Alireza, P. J. Saines, D. A. Tompsett, P. W. Logg, J. Yang, B. Chen, K. Yoshimura, and F. M. Grosche, *Physical Review Letters* **109** (2012), URL <https://doi.org/10.1103/physrevlett.109.237008>.
- [31] S. Goh, D. Tompsett, P. Saines, H. Chang, T. Matsumoto, M. Imai, K. Yoshimura, and F. Grosche, *Physical Review Letters* **114** (2015), URL <https://doi.org/10.1103/physrevlett.114.097002>.
- [32] Y. Wang, S. Yang, P. K. Sivakumar, B. R. Ortiz, S. M. L. Teicher, H. Wu, A. K. Srivastava, C. Garg, D. Liu, S. S. P. Parkin, et al. (2020), arXiv:2012.05898.
- [33] See Supplemental Material for experimental details, sample characterizations under ambient pressure, additional electrical resistivity data under pressure, discussion on persistence of Fermi-liquid behavior under pressure, and pressure-dependence of the upper critical field near the

- low-pressure charge order.
- [34] N. R. Werthamer, E. Helfand, and P. C. Hohenberg, *Phys. Rev.* **147**, 295 (1966), URL <https://link.aps.org/doi/10.1103/PhysRev.147.295>.
- [35] Z. Zhang, Z. Chen, Y. Zhou, Y. Yuan, S. Wang, L. Zhang, X. Zhu, Y. Zhou, X. Chen, J. Zhou, et al. (2021), arXiv:2103.12507.
- [36] X. Chen, X. Zhan, X. Wang, J. Deng, X.-B. Liu, X. Chen, J.-G. Guo, and X. Chen, *Chinese Physics Letters* **38**, 057402 (2021), URL http://cpl.iphy.ac.cn/EN/abstract/article_105899.shtml.